Batteries & Supercaps

Research Article
doi.org/10.1002/batt.202200153

Chemistry Europe
European Chemical Societies Publishing

www.batteries-supercaps.org

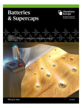

# Ultrathin Magnesium Metal Anode – An Essential Component for High-Energy-Density Magnesium Battery Materialization

Toshihiko Mandai*[a] and Hidetoshi Somekawa[b]

The practical loading, i.e., thickness, of metal anodes predominates the practical energy density of batteries that incorporate elemental metals as anode active materials. Despite its significance for achieving high-energy-density rechargeable magnesium batteries (RMBs), the application of ultrathin magnesium foils remains a challenge because of the brittleness and unworkability of magnesium. This work provides a critical component of a geometric size applicable to laminate-type cells of dimensions 42×32 $mm^2$ or larger. Ultrathin magnesium foil without cracked edges can be fabricated by controlling the initial microstructure. Furthermore, the rolling temperature determines the resulting microstructure and thus the electrochemical properties. The optimal sample, a warm-rolled magnesium foil, exhibited excellent electrochemical characteristics owing to its favorable microstructure, which facilitated a homogeneous distribution of reaction sites. Battery performance using such ultrathin magnesium anodes was investigated with $MgMn_2O_4$ and $\alpha$-$MnO_2$ cathodes. Considering the weights of both the cathodes and anodes, the gravimetric energy density of primitive [$\alpha$-$MnO_2$ || pMg] cells was estimated to be 72 Wh $kg_{electrode}^{-1}$.

## Introduction

Magnesium and its alloys have the lightest densities among conventional metallic materials. The replacement of aluminum-based materials with magnesium-based counterparts offers a potential weight reduction of ca. 20 wt%. However, the practical application of magnesium-based materials is limited because of their crystal structure. Because the von Mises criteria are not satisfied (lack of slip systems) at room and intermediate temperatures, the wrought processability and ductility of magnesium-based materials are inferior to those of competitive lightweight metallic materials, e.g., aluminum alloys. Hence, the fabrication of large components and complicated structures using magnesium-based materials via wrought processes at these temperatures is challenging. As shown in Figure 1(a), a rolled magnesium alloy fabricated using as-cast magnesium (i.e., common rolled magnesium) has many cracked edges. Grain boundaries are a compensation factor in poor slip systems.[1] Several studies on the grain size effect, i.e., the volume fraction of grain boundaries, state that grain refinement effectively enhances ductility and formability.[2,3] Therefore, a high density of grain boundaries plays an important role in resolving the abovementioned intrinsic issues. Birbilis et al. recently fabricated a remarkably thin, formable pure magnesium foil with a thickness of 120 μm by adopting appropriate grain refinement combined with well-controlled rolling processing.[4] Since this pioneering work, 100-μm-thick magnesium foils have appeared on the market.

Such thin magnesium metals are suitable anodes in rechargeable batteries. Rechargeable magnesium batteries (RMBs) are representative energy storage technologies that may help realize an energy-sustainable society.[5] This is because of the natural abundance and favorable electrochemical characteristics of magnesium metal. In principle, its energy density can be increased to 500 Wh $kg^{-1}$ by replacing the graphite anodes of lithium-ion batteries with magnesium metal anodes and applying the redox chemistry of divalent ions to the cathode side.[6] For rechargeable batteries with metal anodes, the thickness and utilization ratio of these anodes strongly affect the energy density. Assuming that the cell capacity and discharge voltage of an ideal stacked cell are fixed at 0.972 Ah and 2.5 V, respectively, and considering the weight/volume of all other cell components (including a separator, current collector, tab, tab lead, pouch foil, and rest space), the gravimetric and volumetric energy densities of a 40-μm-thick magnesium metal anode with a 50% utilization ratio are 186 Wh $kg^{-1}$ and 252 Wh $L^{-1}$, respectively, according to the energy density calculator of Ue et al.[7] The energy densities of cells with the above configuration except the use of a 100-μm-thick magnesium anode at the same utilization as in the former

[a] Dr. T. Mandai
Center for Green Research on Energy and Environmental Materials, Center for Advanced Battery Collaboration
National Institute for Materials Science (NIMS)
1-1 Namiki, Tsukuba, Ibaraki 305-0044, Japan
E-mail: MANDAI.Toshihiko@nims.go.jp

[b] Dr. H. Somekawa
Research Center for Structural Materials
National Institute for Materials Science (NIMS)
1-2-1 Sengen, Ibaraki, 305-0047
Japan

Supporting information for this article is available on the WWW under https://doi.org/10.1002/batt.202200153

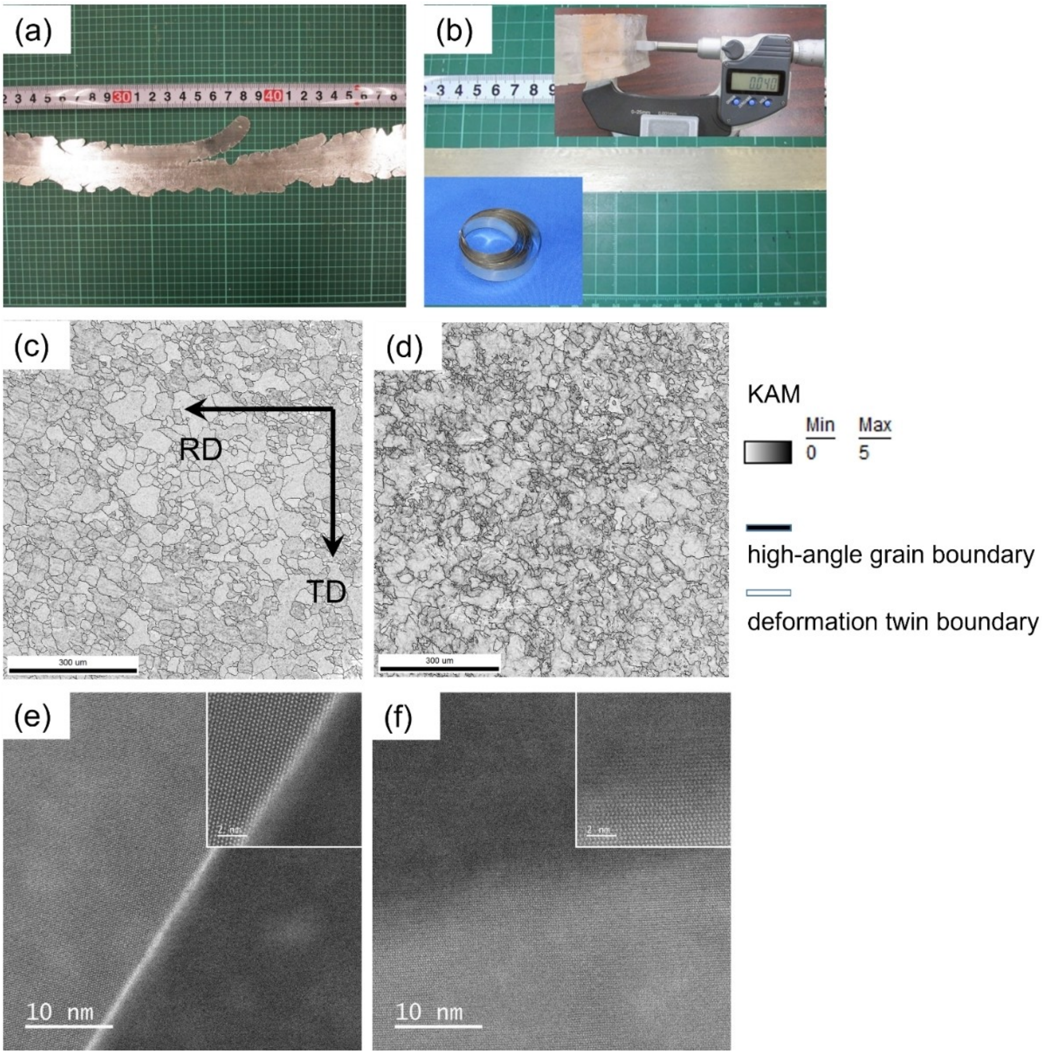


**Figure 1.** Aspects of a) common rolled and b) warm-rolled ultrathin magnesium foil. The common-rolled magnesium foil was obtained by rolling the as-cast magnesium metal as a workpiece. c, d) Kernel Average Misorientation (KAM) maps including grain/twin boundaries and e, f) HAADF-STEM images for c, e) warm-rolled and d, f) cold-rolled magnesium foils. RD is the rolling direction, and TD is the transverse direction. The insets in (e) and (f) are the magnified views.

case, i.e., 20 μm (20%), would be 161 Wh $kg^{-1}$ and 183 Wh $L^{-1}$, respectively. Even a 100-μm-thick magnesium anode is still overloaded relative to present RMB cathodes. The thickness of metal anodes also significantly affects the shape of cell modules. For example, the hardness and brittleness of magnesium metal result in difficulties in fabricating winding-type cells (i.e., 18650-type cells) with thick magnesium metal anodes. The above energy density estimation and such poor formability emphasize that the thickness and metallurgical characteristics of metal anodes should be controlled to produce practical, high-energy-density metal batteries. However, this point is commonly overlooked in the literature.

We fabricate a microstructure-controlled ultrathin magnesium foil and elaborate on its application in RMBs. A ultrathin magnesium foil that has a thickness of $<45$ μm, consists of fine grains, and has few residual stress was successfully fabricated by controlling the initial microstructure of the magnesium billet. This microstructure-controlled ultrathin magnesium foil exhibited superior battery performance compared with the commercially available magnesium alloy foil AZ31 (25–40 μm thickness).[8] This work will pave the way for the application of high-energy-density RMBs.

## Results and Discussion

Commercially cast pure magnesium with a purity of 99.96% was used in this study. The cast magnesium, which had an average grain size of $>100$ μm, was extruded at 423 K at an extrusion ratio of 32:1 to refine its grain structures. This fine-grained extruded magnesium was rolled at 573 K to a thickness of ca. 0.5 mm and then rolled again to form a thin foil at ca. 573 K (warm rolling) and at $<573$ K (cold rolling). The thickness reduction from the first rolling was 15% and that from the second rolling was 1%–2%. The detailed procedure is described in the experimental section. Figure 1(b) displays the warm-rolled magnesium. It had a thickness of ca. 40 μm, width of 30 mm, and length of > 500 mm; it did not have edge cracks and the surface showed a metallic gloss. From a metallurgical viewpoint, the main reason for such sound ultrathin foil fabrication was the control of the initial microstructures before the rolling process. Figure 1(c–f) shows the microstructures of the warm- and cold-rolled foils, observed via the electron backscattering diffraction method and high-angle annular dark-field scanning transmission electron microscopy (HAADF-STEM). Figure 1(c and d) shows kernel average misorientation (KAM) maps, which help identify the magnitude of residual stress; a high KAM value indicates the presence of residual stress. The rolling temperature was found to affect the microstructure. The average grain sizes and average KAM values were 22.2 μm and 0.9°, respectively, for the warm-rolled foil and 13.7 μm and 1.2°, respectively, for the cold-rolled foil. The warm-rolled foil had a coarser average grain size and lower residual stress density than the cold-rolled foil. These microstructural tendencies are consistent with those of wrought-processed metallic materials because the thermomechanical processes at elevated temperatures enhance recrystallization and diffusion. A high density grain boundary generated via extrusion contributes nucleation sites for dislocations during the rolling process. Figure 1(e and f) shows typical atomistic features at high-angle grain boundaries in the warm- and cold-rolled magnesium foils. Regardless of the temperature in the rolling process, the HAADF-STEM images clearly indicate that the high-angle grain boundaries had non-equilibrium interfaces, similar to those in other wrought-processed magnesium alloys.[9] Interestingly, the cold-rolled foil had deformation twin boundaries despite the use of the microstructure-controlled billet, which was associated with the use of low temperatures in the rolling process. Insufficient recrystallization leads to the generation of residual stress and the formation of deformation twins in magnesium and its alloys. The HAADF-STEM images, which show rather blurred grain boundaries, indeed imply insufficient recrystallization in the cold-rolled foil.

The thickness and grain size of the as-fabricated foils were ca. 40 μm and 15–20 μm, respectively; only two or three grains existed in each layer in the cross-sectional direction. It is necessary to determine whether such a relationship between grain size and thickness affects the mechanical properties. Figure S1 (Supporting Information) shows a typical result for the indentation hardness, as obtained from nanoindentation tests at room temperature. The average indentation hardness values were 1.3 and 1.5 GPa for the warm- and cold-rolled foils, respectively. The extruded magnesium with a grain size of 3 μm had an indentation hardness of ca. 0.8 GPa.[10] Common-purity (99.9 %) and ultra-high-purity (99.9999 %) magnesium with fine-grained structures have values of 1–1.5 and 1.5 GPa, respectively.[11] The mechanical properties of pure metals depend on the purity, grain size, and wrought processing method. However, the values obtained for the as-prepared foils were reasonably consistent with the values reported previously. Therefore, thickness was not an influential factor. Furthermore, the cold-rolled foil exhibited superior indentation hardness compared with the warm-rolled foil. This resulted from the fine-grained structure, which is also a general characteristic of metallic materials.

Galvanostatic magnesium deposition-dissolution performance was characterized to assess the usability of the ultrathin magnesium metal foils processed via different thermal treatments as negative electrodes in RMBs. Figure 2 summarizes the cycling profiles of asymmetric [Mg | | Cu] and symmetric [Mg | | Mg] cells employing three different ultrathin magnesium foils. The results for the representative magnesium alloy foil, AZ31 (Mg : Al : Zn = 96 : 3 : 1 by weight, $t$ = 0.03 mm), which was used as a reference system, are provided in Figure S2. As shown in Figure 2(a), the temperature during the rolling process influenced the magnesium deposition-dissolution cycling performance. The warm-rolled foil exhibited a more stable cycling profile over 100 cycles with a remarkably small overpotential (< 30 mV) regardless of whether dissolution or deposition was employed. In contrast, the profile of the foil rolled at low temperatures (cold-rolled) fluctuated and exhibited a greater overpotential, even in the early stages. The cold-rolled sample consisted of relatively fine grains compared with the warm-rolled sample (Figure 1). Grain refinement effectively enhances the electrochemical activities of magnesium metal,[12] so other factors would severely affect their cycling performance.

The larger overpotential of the cold-rolled sample might be due to the localized current density. The KAM maps and HAADF-STEM images of the cold-rolled foil suggest greater residual stress and deformed twins in its microstructure. Such dislocations can promote the uneven utilization of the magnesium anodes. As uneven utilization can lead to nonuniform current distribution, the effective current density of this sample should deviate from the experimental current density estimated simply based on the geometrical surface area of the electrodes, consequently resulting in the unexpectedly large overpotential of the cold-rolled foil during the deposition-dissolution processes. In addition to the overpotential, a typical feature readily attributable to a short circuit phenomenon was clearly observed in the 44th cycle in the cold-rolled sample (Figure 2d). Such a phenomenon is generally caused by a dendrite growth of metal deposits upon repeated deposition-dissolution cycling.[13] Although magnesium deposits are typically spherical (not dendritic) because of their highly passivating nature and the resulting large overpotential for crystallite growth,[14] recent studies show dendrite growth of magnesium.[15,16] Its origin and mechanism have been studied both experimentally and computationally,[17,18] and findings show that the dendrite growth is induced under diffusion-limited conditions. However, the present experimental current density was moderate; hence, the unfavorable dendritic deposition of magnesium should be suppressed. No evidence of dendritic magnesium deposition was found in the cycled magnesium foils (Figure S3). Short circuit characteristics not due to the dendrite growth of deposits have also been recognized in RMB research recently. Our previous work revealed that such “non-dendrite” short circuit phenomena were caused by the penetration of granular deposits in porous separators.[19] Recent systematic studies on magnesium deposition mechanisms further support our argument that three-

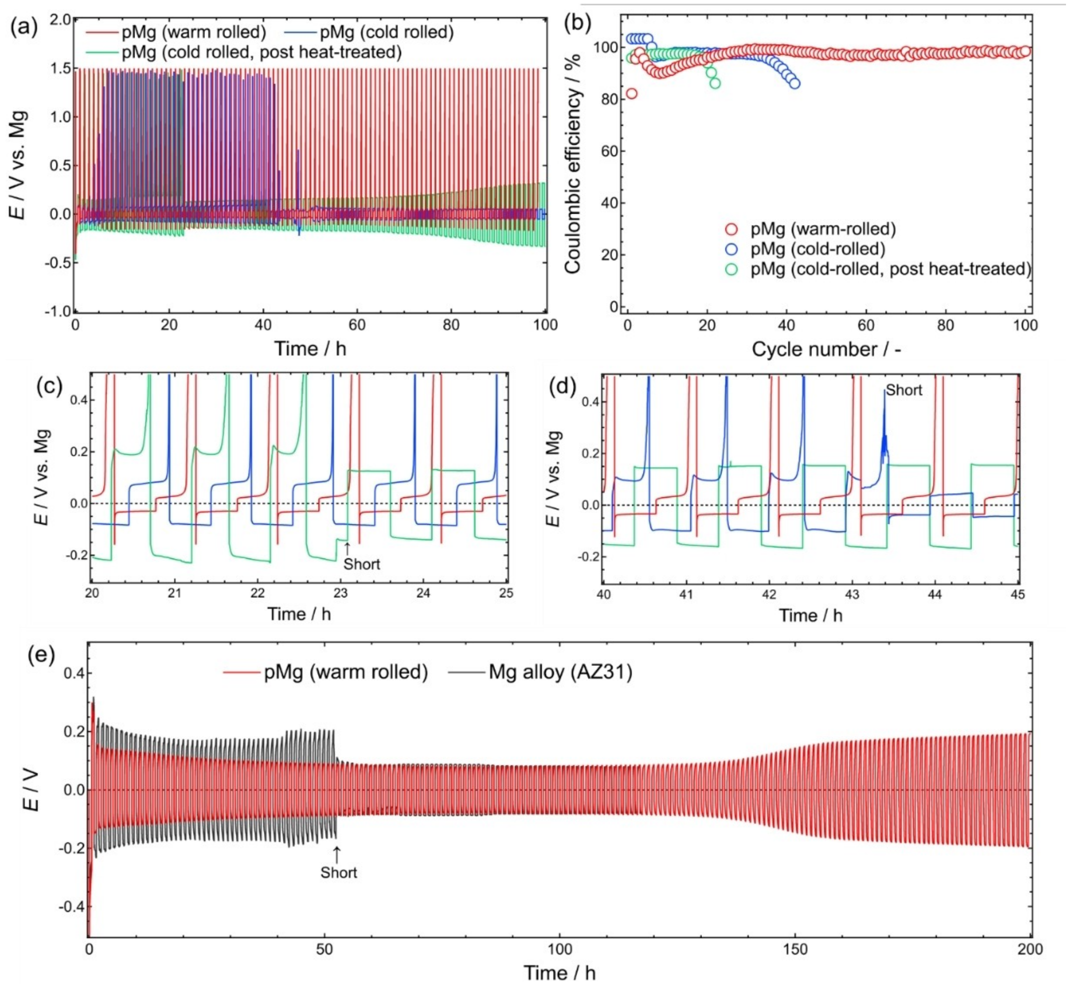


**Figure 2.** a) Galvanostatic magnesium deposition-dissolution cycling profiles and b) corresponding Coulombic efficiency of [pMg | | Cu] cells with ultrathin pMg foils. c, d) Magnified profiles of (a) for selected periods. e) Galvanostatic magnesium deposition-dissolution cycling profiles of symmetric cells with optimal pMg or AZ31 alloy foils.

dimensional magnesium growth arises from mixed kinetic and diffusion control during deposition, and conventional porous separators act as scaffolds for magnesium metal growth.[20] This nondendritic short circuit has been suggested to be further induced by the uneven utilization of magnesium electrodes.[12,19] Comprehensive studies on the relationship between the metallurgical features and electrochemical characteristics of magnesium metal anodes indicate that the free energies of grain boundaries determine the initial electrochemical processes.[12] As shown in Figure 1, greater residual stress was identified, especially at the grain boundaries, in the cold-rolled magnesium foil than in the warm-rolled one. This residual stress originated from dislocations (or defects). Because dislocations are energetically unstable sites, such residual stresses can act as active sites for electrochemical magnesium dissolution. The deformed twin boundaries in the cold-rolled sample could have also enhanced the uneven utilization. Scanning electron microscopy (SEM) images of the cycled magnesium electrodes provide evidence of a rather uneven utilization of the cold-rolled sample compared with the warm-rolled one (Figure S3). Visual observations of separators retrieved from the cells using the cold-rolled magnesium foil also strongly indicated severe penetration of magnesium deposits in the local area corresponding to the reactive sites on the electrodes (Figure S4).

As shown in Figure 2(b), the Coulombic efficiency of the warm-rolled magnesium foil reached a low value in the initial few cycles. Grain boundaries are the starting points of initial electrochemical processes.[12] As the warm-rolled magnesium foil consisted of relatively coarse grains compared with the cold-rolled one, the initial dissolution occurred at limited places where active sites were presented (Figure 3a). The active sites for the subsequent deposition process were located at the perimeters (or edges) of the dissolution pores generated during the initial dissolution process (Figure 3b). The SEM and transmission electron microscopy (TEM) observations of the corresponding cross-sectional views obtained by focused-ion beam (FIB) processing further support this characteristic deposition behavior (Figure S5). After another dissolution on the sample processed with one deposition-dissolution cycle, the resulting surface morphology indicates that both deposited magnesium and the mother magnesium substrate were dissolved during

Research Article
doi.org/10.1002/batt.202200153
Chemistry Europe
European Chemical Societies Publishing

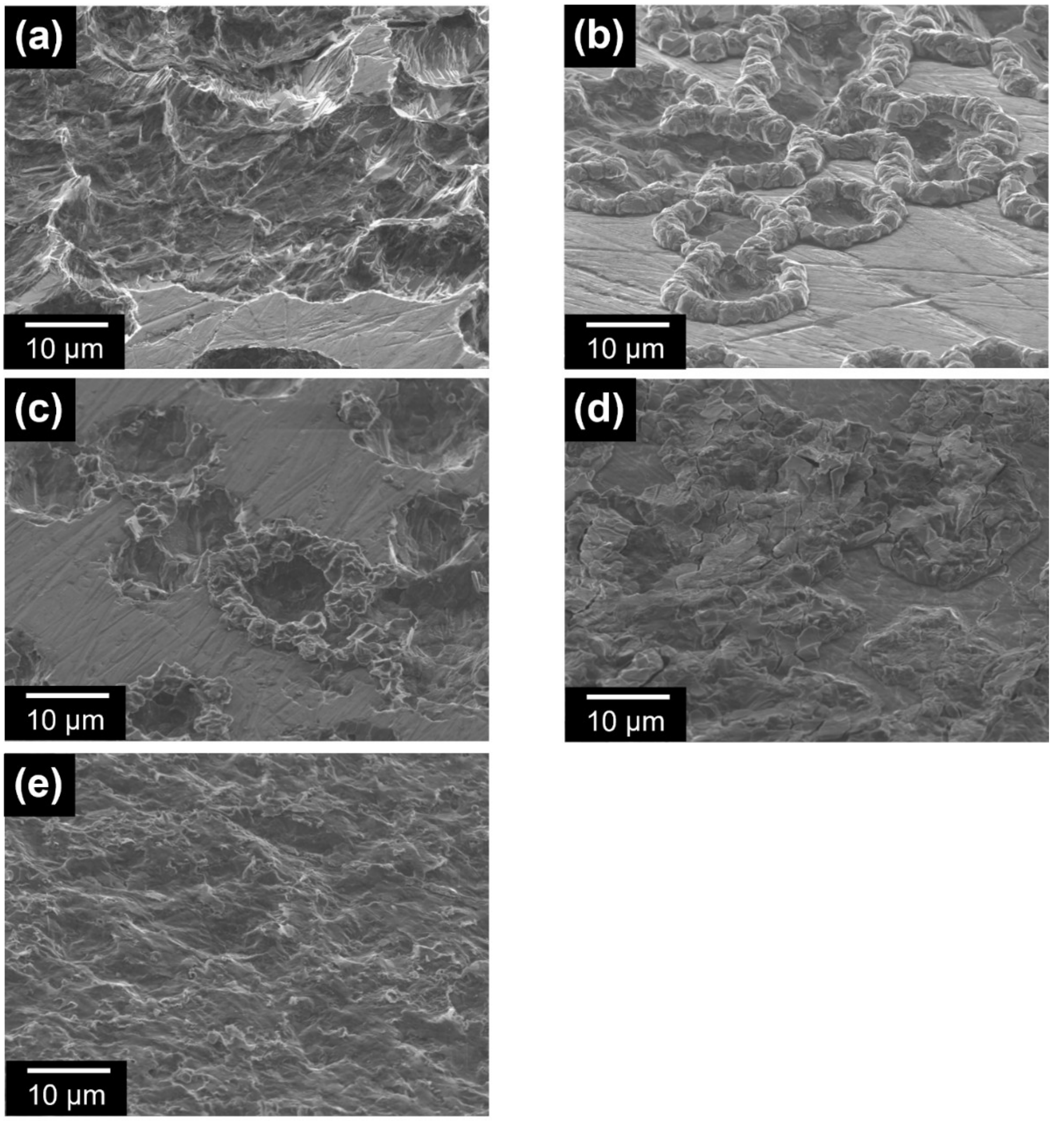


**Figure 3.** Superficial SEM images of warm-rolled magnesium foil after predetermined processes at a current density of 1 mA cm$^{-2}$ for 1 h using 0.3 mol dm$^{-3}$ Mg[B(HFIP)$_4$]$_2$/G2: a) initial dissolution, b) one dissolution-deposition cycle, c) dissolution-deposition-dissolution process, d) two dissolution-deposition cycles, and e) three dissolution-deposition cycles.

this dissolution process (Figure 3c). One additional deposition on the same processed sample also led to site-oriented deposition (Figure 3d). The resulting morphologies after one more dissolution-deposition cycle (total of three cycles) further corroborate an expansion in the utilized area, as shown in Figure 3(e). The active sites in the warm-rolled magnesium electrodes consequently spread throughout the surface upon repeating the dissolution-deposition cycles. During these so-called conditioning processes, each deposition and dissolution was accompanied by some unfavorable side reactions, e.g., electrolyte decomposition. Energy-dispersive X-ray spectroscopy (EDX) analysis results indicate decomposition of the electrolytes (Figure S6). F atoms, attributable to the decomposition products of the electrolytes, were detected mainly around the pores, suggesting that the highly reactive pore sites generated during the conditioning processes could cause a lower-than-unity cycling efficiency. As the number of newly generated pore sites increases with the number of cycles in the initial stages, the Coulombic efficiency may drop to a low value. However, after a certain number of dissolution-deposition cycles, the surface was utilized evenly, and the number of newly generated pore sites consequently decreased. This could lead to the Coulombic efficiency reaching unity. Unlike those in the warm-rolled foil, the active sites in the cold-rolled foil were rather unevenly distributed due to the unfavorable microstructure (Figure S7). The limited sites were indeed utilized during cycling, as depicted in the digital images of the cycled electrodes (Figure S4). Hence, the corresponding Coulombic efficiency could remain high, even in the initial cycles.

Unexpectedly, post-heat treatment further worsened the electrochemical performance (Figure 2). A substantially larger overpotential for both dissolution and deposition was confirmed, and it gradually increased as cycling progressed. In consequence, a parasitic short circuit occurred in the 23rd cycle. As shown in Figure S8, the residual stress significantly decreased upon post-heat treatment but did not completely disappear. Such residual stresses tend to reappear at grain boundaries and each grain interior. SEM images of the cycled foil also demonstrate a characteristic metallurgical structure. Figure S9 suggests that the interior of each grain should be utilized preferentially, resulting in unique petal-like patterns, where the shells of the grains retain their original shapes. However, the post-heat treatment simultaneously induced crystallite growth. A limited part of the electrode surface was utilized locally. Hence, several open holes allowed deposits to penetrate the separator matrix, and a short circuit occurred. The adhered fiber of the separator in the vicinity of the holes strongly supported this observation. These metallurgical characteristics could have led to the notably poor performance of the post-heat-treated cold-rolled sample.

AZ31 alloy, consisting of 96% Mg, 3% Al, and 1% Zn by weight, is a representative anode in magnesium battery applications, and it possesses remarkable formability and acceptable electrochemical properties.[8,21–23] Noked et al. recently reported that the electrochemical characteristics of AZ31 alloy anodes are comparable to those of commercially available 100 μm thick magnesium metal foils.[8] The warm-rolled magnesium foil prepared in this work exhibited superior magnesium dissolution-deposition performance, in terms of both overpotential and Coulombic efficiency, to the AZ31 alloy anode, although relatively stable magnesium dissolution-deposition cycling was achieved using this alloy (Figure S2). The cycling profiles of the symmetric cell further support the better electrochemical performance of the cold-rolled magnesium foil, reaching over 200 cycles with an overpotential of $<80$ mV after the 10 initial cycles of the activation processes, whereas a short circuit occurred in AZ31 (Figure 2e). These interesting characteristics of the warm-rolled sample were also electrolyte independent; highly stable magnesium dissolution-deposition cycling with a small overpotential ($<50$ mV) was achieved, even in a conventional Grignard reagent-based electrolyte (Figure S10). This indicates that the warm-rolled magnesium foil is particularly favorable for electrochemical processes.

The electrochemical performance of the warm-rolled magnesium foil was further assessed through galvanostatic charge-discharge cycling tests with relevant cathode active materials. $MgMn_2O_4$ and $\alpha$-$MnO_2$ cathodes delivered greater initial discharge capacities when combined with the warm-rolled magnesium foil compared with the AZ31 alloy (Figure 4). The profiles of the subsequent cycles also indicate good deliverable capacities and working voltages because of the excellent activities of the warm-rolled magnesium foil.

The warm-rolled magnesium foil can also serve directly as an anode in larger laminate-type cell applications, although the cold-rolled and alloy foils suffered from severe destruction of their physical structures during the ultrasonic welding processes using a Ni tab lead on the foils (Figure S11). The residual stresses and segregation of impurities may direct unfavorable ultrasonic vibrational energies at such active sites, resulting in the possible destruction of the structures. A composite electrode based on magnesium powders is a possible alternative anode to thin magnesium foils for coin-type cell assemblies. However, the structural fragility of such composite electrodes during ultrasonic welding processes would hinder their application to larger laminate-type cells, although they may have superior electrochemical activities compared with bulk magnesium.[24–26] In contrast, the physical appearance of the warm-rolled magnesium foil was stable, even after ultrasonic welding. This metallurgical feature of the warm-rolled magnesium foil is particularly indispensable for fabricating practical magnesium-based batteries without supporting current collectors. This is because the weight of supporting current collectors, e.g., Cu foil, significantly affects the energy densities of the resulting batteries. The cycling performance of the laminate-type cells was comparable to that of conventional test cells (Figure 4; $\phi=16$ mm, electrode area ca. 2.01 $cm^2$); this suggests the presence of well-controlled microstructures, even for the larger electrodes (Figure S12; anode area ca. 13.44 $cm^2$). The gravimetric energy densities of the primitive laminate-type [Mg || $\alpha$-$MnO_2$] cells, considering the weights of a whole cathode (Al foil current collector; $t=10$ μm) and an anode, were calculated to be 72 and 41.6 Wh $kg^{-1}$ for the warm-rolled magnesium foil ($t=40$ μm) and the AZ31 foil ($t=40$ μm) with a

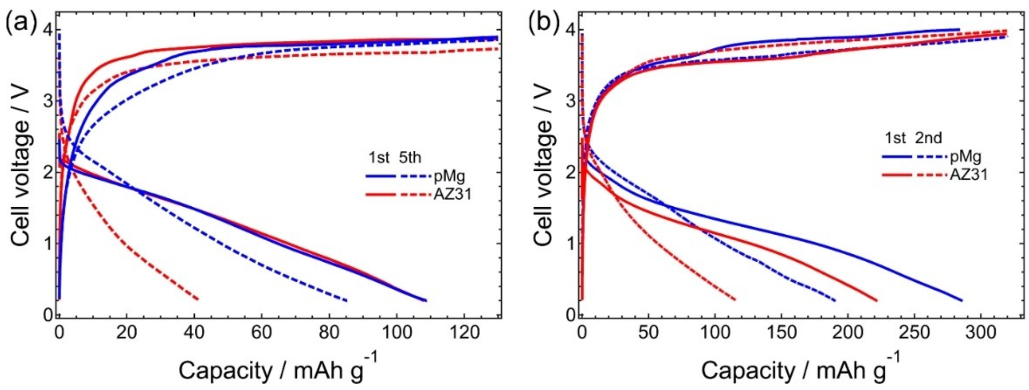


**Figure 4.** Galvanostatic discharge-charge profiles of [pMg or AZ31 || cathode] cells with a) $MgMn_2O_4$ and b) $\alpha$-$MnO_2$ as cathode active materials. Loading: ca. 3 mg $cm^{-2}$, current density: 10 mA $g^{-1}$, temperature: 30 °C.

Research Article
doi.org/10.1002/batt.202200153



supporting Cu current collector ($t = 10\ \mu m$) employed as an anode, respectively.

## Conclusion

We successfully fabricated ultrathin magnesium foil anodes for the first time by controlling the initial microstructure of the extruded magnesium. The rolling temperature had a significant effect on the residual stress in the resulting foil, and rolling at relatively warm temperatures was particularly effective in decreasing the residual stress. This magnesium foil without residual stress exhibited excellent electrochemical properties as an anode in RMB application. Primitive laminate-type cells utilizing the warm-rolled magnesium foil combined with an $\alpha$-$MnO_2$ cathode delivered an initial discharge capacity of $220\ mAh\,g^{-1}$, with an energy density of ca. $72\ Wh\ kg^{-1}$ (estimated considering the weights of both the cathodes and anodes). As the N/P ratio defined by areal capacities of the negative to positive electrodes, was 15 for the present cell (i.e., 15 and $1\ mAh\,cm^{-2}$ for the warm-rolled magnesium anode and the $\alpha$-$MnO_2$ cathode, respectively), a technique for cathode preparation by slurry coating, e.g., $>20\ mg\,cm^{-2}$ loading, and cathode active materials with enhanced battery performance should be developed to achieve practical, high-performance RMBs.

## Experimental Section

### Fabrication of ultrathin magnesium foil

Commercially cast pure magnesium (purity of 99.96%) was used in this study. The cast magnesium, with an average grain size of $>100\ \mu m$, was extruded at 423 K at an extrusion ratio of 32:1 to refine the grain structures. Cast billet was kept in the extrusion furnace at 423 K for at least 30 min and then extruded at a ram speed of $0.2\ mm\,s^{-1}$. The extruded plate was 2 mm thick, 30 mm wide, and $>100$ cm long. This extruded magnesium was cut to a length of 120 mm and kept in the furnace at 573 K for 10 min. Then, this plate was rolled at a setting temperature of 573 K with a thickness reduction of 15% (ca. 0.5 mm). The rolled sheet was reheated at every pass at 573 K for 3 min to prevent heat removal during the rolling process. The rolled magnesium was again rolled into a foil at ca. 573 K (warm rolling) and at ca. 523 K (cold rolling). In the second rolling process, the thickness reduction was between 1% and 2% in each case. Reheating was performed for 60 s every two passes to a thickness of 0.2 mm (for the warm-rolled sample) and for 60 s every 10 passes to a thickness of 0.1 mm (for the cold-rolled sample) in the second rolling process. The major reason for the rolling temperature of 573 K was that the basal and nonbasal planes for dislocation slip show similar critical resolved shear stress. This suggests that the von Mises criteria are satisfied at this temperature.

### Indentation hardness

Hardness properties were measured via the nanoindentation method (Hysitron, TriboIndenter) under open-loop conditions at room temperature. The maximum load was set to 1 mN, and the loading and unloading rates were 1 mN/s. A conical tip was used to ignore the microstructural evolution, i.e., to prevent deformation twin formation during the indentation tests. The measurement point in each test was $>100$. Sample preparation for the nano-indentation tests was the same as that for the initial microstructural observations using EBSD.

### Electrochemical characterization

Electrochemical magnesium dissolution/deposition characteristics were evaluated through galvanostatic cycling measurements using asymmetric and symmetric two-electrode assemblies with an automatic charge-discharge instrument (HJ0610SD8Y, Hokuto-Denko Co., Ltd.). For the asymmetric cells, mechanically polished Mg and Cu foils, a glass fiber filter (GF/A; $t = 0.26$ mm, Whatman), and $0.3\ mol\,dm^{-3}$ $Mg[B(HFIP)_4]_2$/G2 (HFIP is hexafluoroisopropoxyl; G2 is diglyme) served as working and counter electrodes, a separator, and an electrolyte, respectively. The electrolyte was synthesized according to a previously reported procedure.[19,27] A current density of $1\ mA\,cm^{-2}$ for 30 min for each dissolution and deposition at 30 °C was adopted for both the symmetric and asymmetric assemblies. Galvanostatic discharge-charge cycling was also performed on the [pMg or AZ31 alloy | $0.3\ mol\,dm^{-3}$ $Mg[B(HFIP)_4]_2$/G2 | $MgMn_2O_4$ or $\alpha$-$MnO_2$] cells. Coin-type cells ($\phi = 16$ mm; $2.01\ cm^2$) and laminate-type cells ($40\times30$ and $42\times32\ mm^2$ for cathode and anode, respectively) were fabricated for use in this study. The cathode active materials, $MgMn_2O_4$ and $\alpha$-$MnO_2$, were synthesized via the well-established sol-gel method and hydrothermal treatment.[28,29] The cathode slurry was prepared by mixing the active material, carbon nanotube as conducting support, and polyvinylidene difluoride (PVdF) as a binder (92:4:4 in weight fraction) with an appropriate amount of *N*-methyl-2-pyrrolidone as a dispersant. The slurry was spread on an Al current collector and then dried under vacuum heating at 80 °C for 12 h. The dried composite sheets were compressed with a roll press and cut into circular or rectangle shapes with dimensions of $\phi = 16$ mm or $40\times30\ mm^2$, respectively. For the laminate-type cells, a Ni tab was placed on each cathode and anode via ultrasonic welding. As a reference anode sample, ultrasonic welding was attempted for the cold-rolled magnesium foil and AZ31 alloy. The battery cells were assembled by using the composite cathode, Mg anode, a glass fiber separator, and $0.3\ mol\,dm^{-3}$ $Mg[B(HFIP)_4]_2$/G2 electrolyte. The cycling test was performed in the voltage range of 0.2–4 V at 30 °C with a current density of $10\ mA\,g^{-1}$, regardless of the used cathode active materials.

### Microstructure observation

The initial microstructures of the warm- and cold-rolled magnesium foils were observed via electron backscatter diffraction (EBSD) in EDAX/TSL. The samples for EBSD observation were mechanically polished to a mirror surface with a SiC paper, 6 and 1 μm diamond suspensions, and colloidal silica slurry. They were subsequently polished with an acid solution. The data were then analyzed using EDAX (version 7).

The atomistic features of the high-angle grain boundaries of the warm- and cold-rolled magnesium foils were observed via high-resolution transmission electron microscopy (HRTEM; JEM-ARM200F). The observed plane was perpendicular to the rolling direction, i.e., normal and transverse directions. The HRTEM samples were subjected to FIB processing.

The surfaces of the cycled magnesium anodes were observed via SEM (JSM-7800F, JEOL) and TEM (JEM-ARM200F) and subsequently characterized through EDX. The samples were washed with anhydrous THF to remove the residual electrolytes, dried under high-vacuum conditions, placed in an airtight chamber, and transferred for SEM and TEM observations without exposure to air.

## Supporting Information

General experimental details and characterization data are included in the Supporting Information.

## Author Contributions

Toshihiko Mandai: data curation, formal analysis, resources, investigation, funding acquisition, project administration, writing-original draft, review, and editing. Hidetoshi Somekawa: conceptualization, data curation, formal analysis, resources, investigation, funding acquisition, project administration, writing-review and editing.

## *Acknowledgements*

*We thank Ms. Makiko Oshida and Mr. Keisuke Shinoda for their kind support on a series of microscopy observations and CP and FIB processing at the NIMS Battery Research Platform. The cathode active materials of $MgMn_2O_4$ and $\alpha$-$MnO_2$ were kindly supplied by Prof. Imai at Keio University and Prof. Kanamura at Tokyo Metropolitan University, respectively. This work was financially supported by the Advanced Low-Carbon Technology-Specially Promoted Research for Innovative Next Generation Batteries Program (ALCA-SPRING, Grant Number JPMJAL1301) and the NEXT Center of Innovation Program (COI-NEXT, Grant Number JPMJPF2016) of the Japan Science and Technology Agency.*

## *Conflict of Interest*

The authors declare no conflict of interest.

## Data Availability Statement

The data that support the findings of this study are available from the corresponding author upon reasonable request.

**Keywords:** energy density · magnesium anode · metallurgy · residual stress · thin electrode

[1] J. Koike, *Metal. Mater.* **2005**, *36a*, 1689–1696.
[2] H. Somekawa, *Mater. Trans.* **2020**, *61*, 1–13.
[3] H. Somekawa, A. Kinoshita, A. Kato, *Mater. Sci. Eng.* **2016**, *A676*, 427–433.
[4] Z. Zeng, J. F. Nie, S. W. Xu, C. H. J. Davies, N. Birbilis, *Nat. Commun.* **2017**, *8*, 972.
[5] H. D. Yoo, I. Shterenberg, Y. Gofer, G. Gershinsky, N. Pour, D. Aurbach, *Energy Environ. Sci.* **2013**, *6*, 2265–2279.
[6] I. D. Johnson, B. J. Ingram, J. Cabana, *ACS Energy Lett.* **2021**, *6*, 1892–1900.
[7] M. Ue, K. Uosaki, *Curr. Opin. Electrochem.* **2019**, *17*, 106–113.
[8] A. Maddegalla, A. Mukherjee, J. A. Blázquez, E. Azaceta, O. Leonet, A. R. Mainar, A. Kovalevsky, D. Sharon, J. F. Martin, D. Sotta, Y. E. Eli, D. Aurbach, M. Noked, *ChemSusChem* **2021**, *14*, 4690–4696.
[9] H. Somekawa, K. Naito, H. Watanabe, *Materialia* **2020**, *14*, 100947.
[10] H. Somekawa, C. A. Schuh, *Acta Mater.* **2011**, *59*, 7554–7563.
[11] H. Somekawa, J. Yi, A. Singh, K. Tsuchiya, *Mater. Sci. Eng.* **2021**, *A823*, 141735.
[12] T. Mandai, H. Somekawa, *Chem. Commun.* **2020**, *56*, 12122–12125.
[13] X. Zhang, A. Wang, X. Liu, J. Luo, *Acc. Chem. Res.* **2019**, *52*, 3223–3232.
[14] M. Matsui, *J. Power Sources* **2011**, *196*, 7048–7055.
[15] M. S. Ding, T. Diemant, R. J. Behm, S. Passerini, G. A. Giffin, *J. Electrochem. Soc.* **2018**, *165*, A1983–A1990.
[16] R. Davidson, A. Verma, D. Santos, F. Hao, C. Fincher, S. Xiang, J. V. Buskirk, K. Xie, M. Pharr, P. P. Mukherjee, S. Banerjee, *ACS Energy Lett.* **2019**, *4*, 375–376.
[17] R. Davidson, A. Verma, D. Santos, F. Hao, C. D. Fincher, D. Zhao, V. Attari, P. Schofield, J. V. Buskirk, A. F. -Cartagena, T. E. G. Alivio, R. Arroyave, K. Xie, M. Pharr, P. P. Mukherjee, S. Banerjee, *Mater. Horiz.* **2020**, *7*, 843–854.
[18] A. Hagopian, D. Kopač, J.-S. Filhol, A. K. Lautar, *Electrochim. Acta* **2020**, *353*, 136493.
[19] T. Mandai, *ACS Appl. Mater. Interfaces* **2020**, *12*, 39135–39144.
[20] J. E. -Rathert, K. Moyer, M. Zohair, C. L. Pint, *Joule* **2020**, *4*, 1324–1336.
[21] T. Mandai, Y. Akita, S. Yagi, M. Egashira, H. Munakata, K. Kanamura, *J. Mater. Chem. A* **2017**, *5*, 3152–3156.
[22] T. Mandai, K. Tatesaka, K. Soh, H. Masu, A. Choudhary, Y. Tateyama, R. Ise, H. Imai, T. Takeguchi, K. Kanamura, *Phys. Chem. Chem. Phys.* **2019**, *21*, 12100–12111.
[23] M. Shimizu, A. Nakahigashi, S. Arai, *Phys. Chem. Chem. Phys.* **2021**, *23*, 16981–16988.
[24] Y. Liang, R. Feng, S. Yang, H. Ma, J. Liang, J. Chen, *Adv. Mater.* **2011**, *23*, 640–643.
[25] J. Bitenc, K. Pirnat, T. Bančič, M. Gaberšček, B. Genorio, A. R. -Vitanova, R. Dominko, *ChemSusChem* **2015**, *8*, 4128–4132.
[26] P. Wang, J. Trück, S. Niesen, J. Kappler, K. Küster, U. Starke, F. Ziegler, A. Hintennach, M. R. Buchmeiser, *Batteries & Supercaps* **2020**, *3*, 1239–1247.
[27] T. Mandai, Y. Youn, Y. Tateyama, *Mater. Adv.* **2021**, *2*, 6283–6296.
[28] K. Sone, Y. Hayashi, T. Mandai, S. Yagi, Y. Oaki, H. Imai, *J. Mater. Chem. A* **2021**, *9*, 6851–6860.
[29] R. Ma, Y. Bando, L. Zhang, T. Sasaki, *Adv. Mater.* **2004**, *16*, 918–922.

Manuscript received: March 31, 2022
Revised manuscript received: May 25, 2022
Accepted manuscript online: May 26, 2022
Version of record online: June 14, 2022